Supporting Information

Milton et al. 10.1073/pnas.1014511108

SI Materials and Methods

***Drosophila* Strains and Genetic Controls.** We used the following strains in our analyses: *spin*^{4} and *spin*^{5} (1), *sod1*^{n1}, *sod1*^{n64}, *sod2*$^{\Delta 12}$, *sod2*$^{\Delta 02}$, UAS-*JNK*$^{[K53R]}$, UAS-*fos*^{DN} UAS-*jun*^{DN} (2, 3), *atg1*$^{[003051]}$, *atg1*$^{[DG23110]}$, *atg18*$^{[KG03090]}$, *Df(3L)Exel6112/TM6b*, *puc*^{E69}, *MHC*-GAL4, and *ElaV*-GAL4(3E1) (Bloomington Stock Center), *spin*GAL4, *spin*$^{\Delta 58}$ (Daisuke Yamamoto, Tohoku University, Sendai, Japan) (4), UAS-*hSOD1*, UAS-*cat*, and UAS-*TrxR1* (Fanis Missirlis, Queen Mary's University, London, UK), UAS-atg5IR (Manolis Fanto, King's College, London, UK), UAS-*ASK1*^{DN} (Masayuki Miura, University of Tokyo, Tokyo, Japan) (5), *hiw*^{ND9} (Aaron DiAntonio, Washington University, St. Louis, MO) (6), and *gst-D*-GFP (Dirk Bohmann, University of Rochester, Rochester, NY) (7).

Fly Husbandry. Flies were kept on standard yeast, sugar, and agar mix at 25 °C. Paraquat treatment: first-instar larvae were transferred to formula 424 instant *Drosophila* medium with yeast and (Carolina Biological Supply Company) made up with an equal volume of water containing paraquat (Sigma).

Immunocytochemistry. Wandering third-instar larvae were dissected and stained as described previously (1). Fly adult brains were dissected in 4% formaldehyde/PBS and stained with nc82 antibody (Developmental Studies Hybridoma Bank). Brains were processed identically to third-instar larvae. β-Gal induction was imaged using rabbit anti-LacZ (Cappel; 1/1,000), control larvae being stained in the same solutions as the experimental larvae.

Imaging and Quantification. Bouton number at muscle 6/7 of segment A3 was determined by counting every distinct spherical anti-syt stained varicosity along the motor neuron at the muscle. Muscle surface area was calculated by imaging muscle 6/7 with a Leica DC500 digital camera with a Leica DMLA microscope and calculating the size using ImageJ. For Figs. S3 and S4, data are presented as raw bouton number, muscle surface area, and bouton number normalized to wild-type muscle surface area. This division is because of the smaller developmental size of the *sod1*, *sod2*, and paraquat-treated animals. Bouton numbers were normalized by dividing the bouton number by the muscle surface area and multiplying by mean wild-type muscle surface area. In experiments involving *spin* and *hiw* mutants, muscle surface area was always found to be identical to wild-type so normalization was deemed unnecessary. In sod1 and sod2 mutants, muscle fibers are smaller than wild-type, although we present our data as raw bouton number. This analysis represents an underestimate of synaptic overgrowth in these animals. We present in Fig. S2 the bouton number, as raw bouton counts, muscle surface area, and normalized to wild-type muscle surface area. In paraquat-treated animals, muscle surface area was seen to vary, and normalization was carried out. Bouton size was measured as width across the bouton at the widest point, using imageJ and images taken with a 63× objective. Branching number was quantified as the number of divergent points on the synaptic arbor. Confocal images were obtained in LSM510; Carl Zeiss using Plan-Apochromat 63× NA 1.4 oil differential (for neuromuscular junctions, NMJs), 40× for anti-lacZ; the same settings were used for experimental and control images.

Lipid Peroxidation Assay. Five-day-old flies were collected and stored at −80 °C. Thirty flies were used for Bioxytech LPO-586 assay (Oxis Research). Flies were homogenized in ice-cold PBS/5 mM butylated hydroxytoluene, centrifuged at 3,000 × *g* at 4 °C for 10 min. A 200-μL sample was added to 650 μL diluted R1 (*N*-methyl-2-phenylindole in acetonitrile with ferric iron in methanol), mixed, 150-μL concentrate HCl then added, and incubated at 45 °C for 60 min. Absorbance at 586 nm was recorded (OD meter) and compared with standards of tetramethoxypropane.

Fluorimetry. Whole flies were collected, homogenized on ice in 10 μL per animal of lysis buffer [150 mM NaCl, 20 mM Tris pH8, 2 mM EDTA, 0.5% Igepal with protease inhibitor (Roche)], incubated on ice for 15 min, and spun at 4 °C at 21,000 × *g* for 10 min, the supernatant spun again for 15 min at 21,000 × *g* at 4 °C. Next, 300 μL PBS was added to the supernatant and fluorescence measured using a Fluoromax-4 spectrofluorometer. The settings used were: excitation 480 nm and emission recorded between 490 and 600 nm. Similar protein concentrations were confirmed by Bradford Assay.

Electrophysiology. Wandering third-instar larvae were dissected in modified HL3 (8). Modified HL3 composition is as follows: NaCl (110 mM), KCl (5 mM), $NaHCO_3$ (10 mM), Hepes (5 mM), sucrose (30 mM), trehalose (5 mM), $CaCl_2$ (1 mM), and $MgCl_2$ (20 mM) (pH 7.2). Intracellular recordings were made in muscle 6 from either segment A3 or A4. A suction electrode was used to stimulate motorneurons at 10 Hz for 10 min. The first 100 excitatory junction potentials were averaged and this value was used to normalize excitatory junction potentials recorded in each individual larva. Graphs show the first 100 stimulations and then averages of 100 stimulations thereafter; every other datapoint is plotted for clarity. Error bars are SEM. There was no significant difference ($P > 0.05$) in either resting membrane potentials or input resistances in any of the genotypes from which they were recorded.

1. Sweeney ST, Davis GW (2002) Unrestricted synaptic growth in *spinster*-a late endosomal protein implicated in TGF-β-mediated synaptic growth regulation. *Neuron* 36:403–416.
2. Rowland AM, Richmond JE, Olsen JG, Hall DH, Bamber BA (2006) Presynaptic terminals independently regulate synaptic clustering and autophagy of GABAA receptors in *Caenorhabditis elegans*. *J Neurosci* 26:1711–1720.
3. Sanyal S, Sandstrom DJ, Hoeffer CA, Ramaswami M (2002) AP-1 functions upstream of CREB to control synaptic plasticity in *Drosophila*. *Nature* 416:870–874.
4. Nakano Y, et al. (2001) Mutations in the novel membrane protein *spinster* interfere with programmed cell death and cause neural degeneration in *Drosophila melanogaster*. *Mol Cell Biol* 21:3775–3788.
5. Bamber BA, Rowland AM (2006) Shaping cellular form and function by autophagy. *Autophagy* 2:247–249.
6. Wan HI, et al. (2000) Highwire regulates synaptic growth in *Drosophila*. *Neuron* 26: 313–329.
7. Sykiotis GP, Bohmann D (2008) Keap1/Nrf2 signaling regulates oxidative stress tolerance and lifespan in *Drosophila*. *Dev Cell* 14:76–85.
8. Dermaut B, et al. (2005) Aberrant lysosomal carbohydrate storage accompanies endocytic defects and neurodegeneration in *Drosophila benchwarmer*. *J Cell Biol* 170: 127–139.

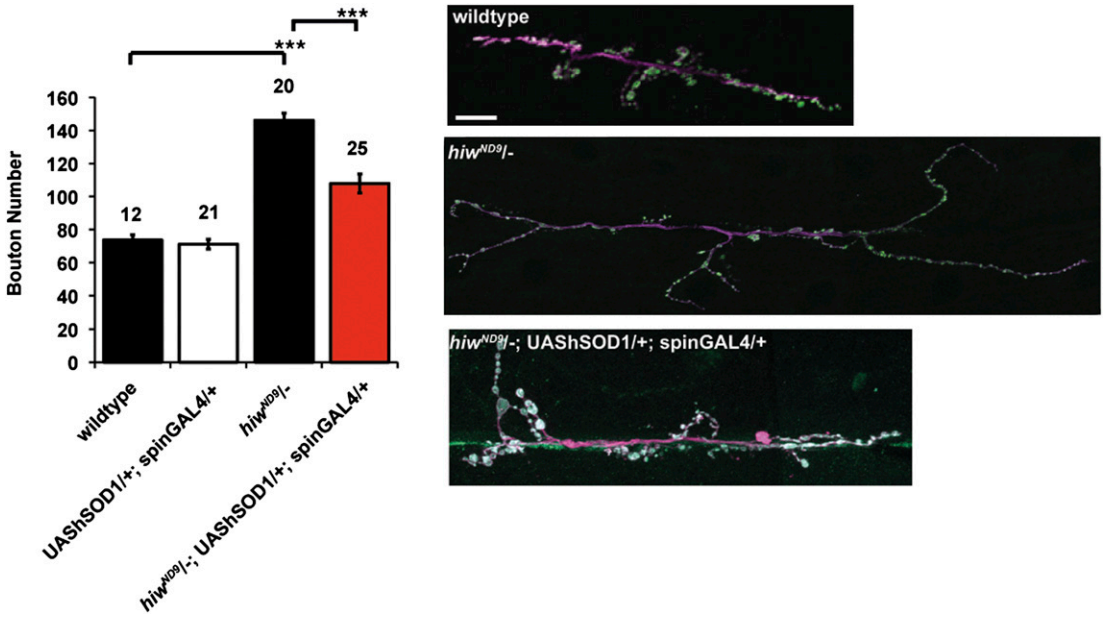

Fig. S1. Overexpression of antioxidant transgenes partially rescues *hiw* induced overgrowth. Mutations in *hiw* cause a significant increase in bouton number to 146 ± 5.7 (n = 20) compared with wild-type 74 ± 3.2 (n = 12). Expression of *hSOD1* using *spin*GAL4 reduces bouton number in *hiw* to 108 ± 5.90 (n = 25), significantly different from *hiw* (***$P < 0.001$, ANOVA).

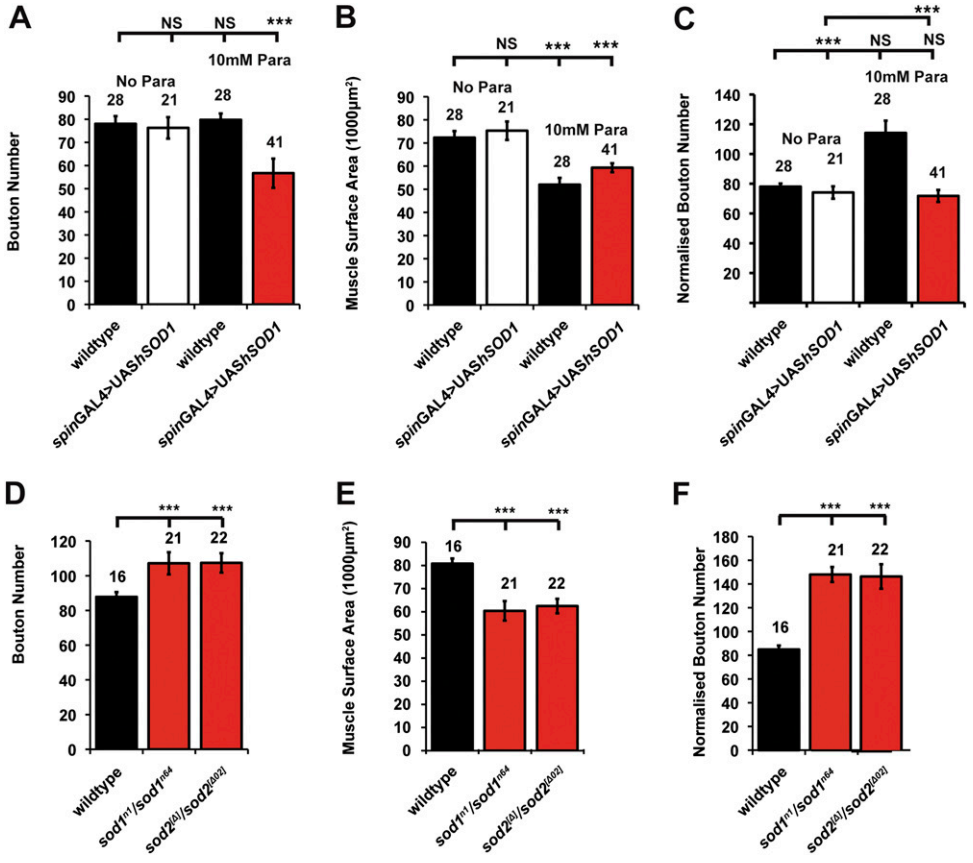

Fig. S2. Paraquat feeding and mutants defective for oxidative stress (OS) defense have increased synaptic growth compared with controls. Feeding larvae on 10-mM paraquat results in smaller larvae entering the third-instar stage of development. We present the data here as raw bouton number (*A*), muscle surface area (to demonstrate reduction in size) (*B*), and bouton number normalized to wild-type muscle surface area (*C*). (*A*) Paraquat feeding (10 mM) generates larvae with an average raw bouton number of 80 ± 6.64 (n = 41) compared with animals reared on paraquat expressing UAS-*hSOD1* simultaneously in nerves and muscles (using *spin*GAL4) with a raw bouton number 57 ± 2.64 (n = 21) (***$P < 0.001$, ANOVA). Overexpression of *hSOD1* in the absence of paraquat did not significantly change raw bouton number (76 ± 5.56, n = 21) compared with wild-type (78 ± 2.14 n = 28, $P > 0.05$, ANOVA). (*D*) Mutations in *sod1 and sod2* have bouton numbers of 107 ± 4.8 (n = 21) and 107 ± 4.9 (n = 22), significantly larger than wild-type synapses, bouton number 85 ± 3.3 (n = 16) (***$P < 0.001$, ANOVA). (*E*) Mutations in *sod1* and *sod2* also cause a significant reduction in muscle surface area from wild-type 80,801 μm² ± 2,264 (n = 16) to 60,421 μm² ± 4,218 (n = 21) and 62,478 μm² ± 3,136 μm² (n = 22), respectively (***$P < 0.001$, ANOVA). (*F*) Mutations in *sod1* and *sod2* cause significantly overgrown NMJs. Wild-type larvae have a mean bouton number of 85 ± 3.3 (n = 16), which is increased by mutations in *sod1* to 147 ± 6.3 (n = 21) and *sod2* to 146 ± 10.6 (n = 22) normalized to wild-type muscle surface area (***$P < 0.001$, ANOVA). Error bars show SEM and the black numbers above each bar is the n value. Following normalization, both mutations cause a significant increase in bouton number.

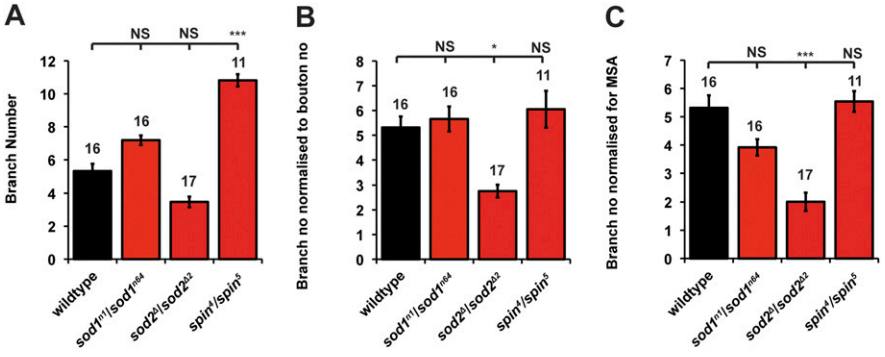

Fig. S3. Increases in branching are generally proportional to increases in bouton number. (*A*) *spinster* has significantly increased branching (***$P < 0.001$, ANOVA) 10.8 ± 1.37 (n = 11) compared with wild-type 5.3 ± 0.44 (n = 16). *sod1* and *sod2* are not significantly different in this statistical test, with branch number of 7.2 ± 0.64 (n = 16) and 3.5 ± 0.32 (n = 17). (*B*) When normalized to bouton number, *sod1* and *spinster* branch numbers are not statistically different from wild-type; 5.66 ± 0.5 (n = 16) and 6.1 ± 0.74 (n = 17), respectively, ($P > 0.05$, ANOVA). *sod2* has a significantly decreased branch number 2.8 ± 0.26 (n = 17) (*$P < 0.05$, ANOVA) (*C*) The same pattern is seen when bouton number is normalized to allow for muscle surface area, thus accounting for muscle surface area. *sod1* and *spinster* do not have statistically different branch number 3.92 ± 1.75 (n = 16) and 5.54 ± 2 (n = 16) ($P > 0.05$, ANOVA); *sod2* has significantly reduced branching, 2.01 ± 1.4 (n = 17) (***$P < 0.001$, ANOVA).

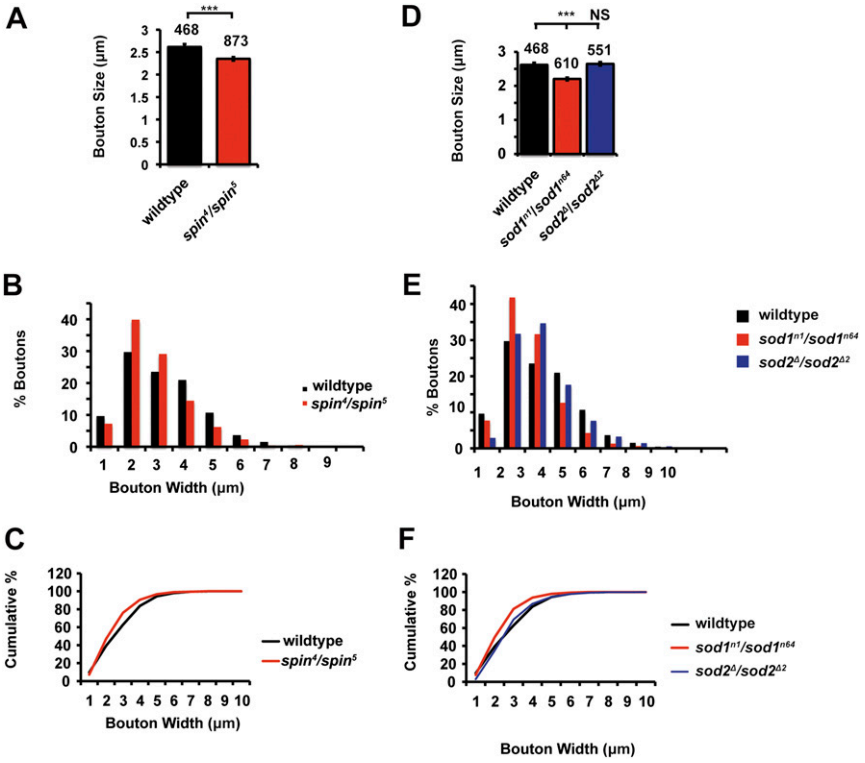

Fig. S4. OS causes changes in bouton size. (*A*) *spinster* has smaller boutons than wild-type mean bouton width in wild-type is 2.6 ± 0.06 (n = 468) and 2.35 ± 0.04 (n = 873) (***$P < 0.001$, Student t test). (*B*) Bouton size in *spinster* is also displayed as percentage of boutons at each micrometer width; the distribution of bouton size is significantly different, with *spinster* showing a higher proportion of smaller boutons (***$P < 0.001$, Kolmogorov-Smirnov). (*C*) Cumulative percentage of bouton numbers at each micrometer width in wild-type and *spinster* showing the difference in distribution. (*D*) *sod1* has a significantly reduced mean bouton width compared with wild-type: reduced from 2.62 ± 0.064 (n = 468) in wild-type to 2.2 ± 0.042 (n = 610) (***$P < 0.001$, ANOVA). *sod2* mutants have a mean bouton width of 2.65 ± 0.053, not statistically different from wild-type ($P > 0.05$, ANOVA). (*E*) The percentage of boutons in at each micrometer width, showing the increased proportion of smaller boutons in *sod1*; this difference in distribuion is significant (***$P < 0.001$, Kolmogorov-Smirnov). The *sod2* mutants also show a difference in the distribution of bouton sizes (***$P < 0.001$, Kolmogorov-Smirnov), with an increased proportion of larger boutons. (*F*) Graph shows the cumulative percentage of boutons in each micrometer width.

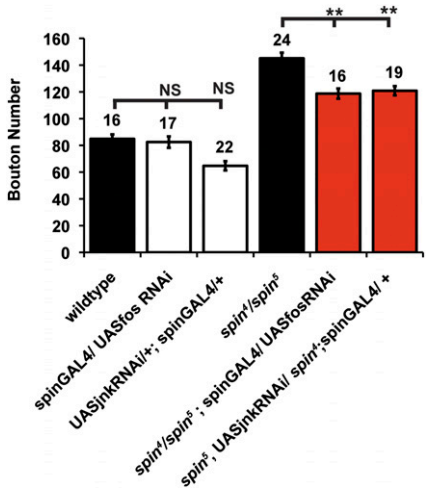

Fig. S5. Depleting JNK/AP-1 signaling through expression of RNAi transgenes pre- and postsynaptically rescues *spin*-induced synaptic overgrowth. Expression of *fos*-RNAi or *jnk*-RNAi in *spin* significantly reduces raw bouton number overgrowth from 145 (n = 24) to 119 (n = 16) and 121 (n = 19), respectively (**$P < 0.01$, ANOVA).

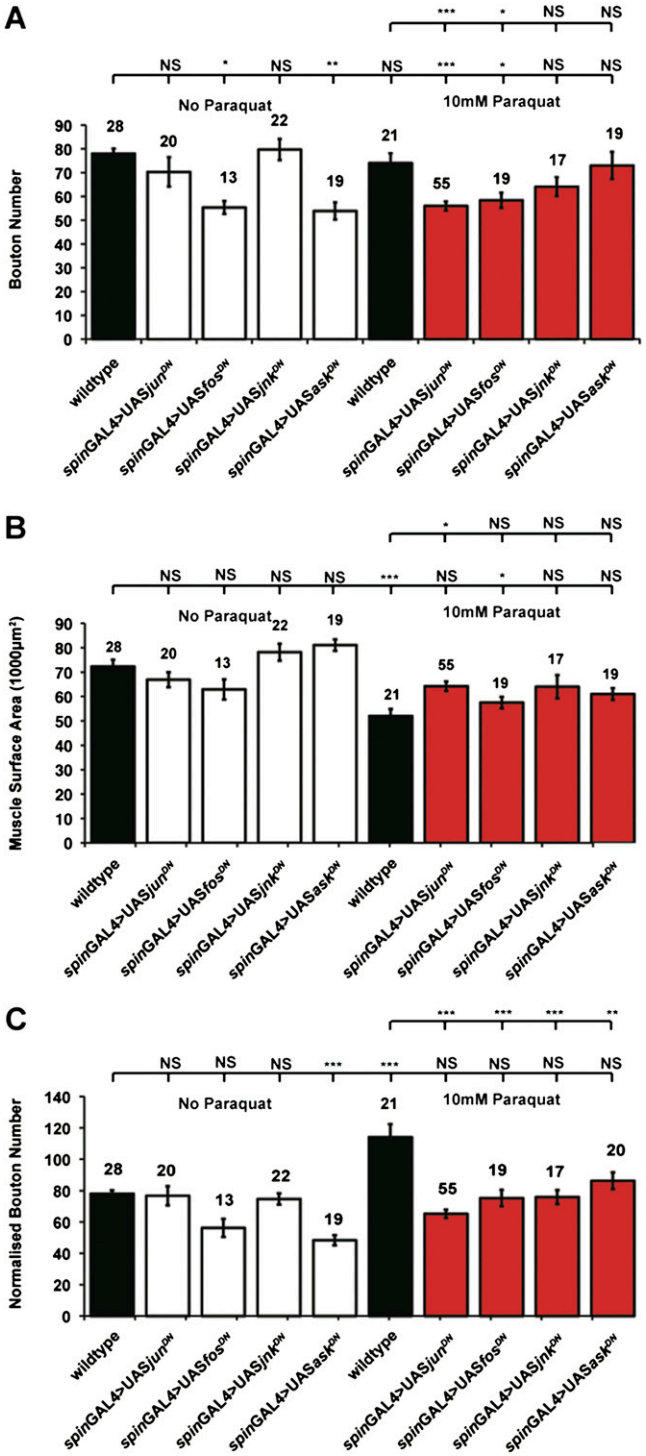

Fig. S6. Paraquat-induced increase in bouton number is significantly reduced by depleting ASK/JNK/AP1 signaling. (*A*) Expression of fos and jun dominant-negative transgenes pre- and postsynaptically (under the control of spinGAL4) in animals fed on paraquat significantly reduces the increase in raw bouton number (jun^{DN} ***$P < 0.001$, fos^{DN} *$P < 0.05$, ANOVA). Expression of jun^{DN} in animals fed on 10-mM paraquat caused a reduction in raw bouton number from a wild-type of 80 ± 6.64 (n = 22) to 56 ± 1.93 (n = 55). (*C*) When normalized to (nonparaquat-treated) wild-type muscle surface area (expressed in *B*), the paraquat-treated wild-type bouton count is 114 ± 8.26 and jun^{DN} expression reduces bouton number to 65 ± 2.64. Similarly, fos^{DN} expression reduced raw bouton number from 80 ± 6.64 (n = 22) to 55 ± 2.7 and normalization reveals a difference in bouton number of 114 ± 8.26 (n = 22) to 56 ± 5.77 (n = 13). When normalized to wild-type muscle surface area, expression of JNK^{DN} and ASK^{DN} causes significant reduction in paraquat-induced bouton number from 114 ± 8.26 (n = 22) to 76 ± 4.49 (n = 17) and 86 ± 7.81 (n = 19), respectively (***$P < 0.001$ and **$P < 0.05$, respectively, ANOVA).

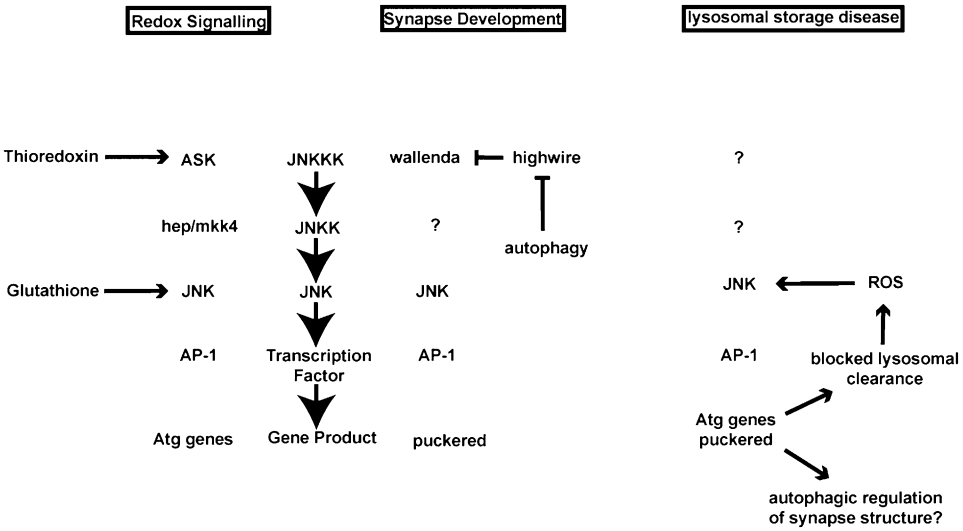

Fig. S7. OS induces synapse development by activation of the JNK/AP-1 pathway. The JNK signaling pathway is well known to regulate many aspects of synapse development and function (1–4), although the transcriptional targets of AP-1 that regulate synapse growth have yet to be identified. Up-regulation of the pathway promotes synapse growth, as shown in *hiw* mutants, where wallenda signaling is unrestrained, leading to overgrown NMJs via activation of fos (3). Furthermore, hiw levels are controlled by autophagy, thus in wild-type animals increasing autophagy leads to decreased levels of hiw, resulting in NMJ overgrowth (5). The synaptic overgrowth in hiw mutants is seen to be independent of autophagy, although the genes up-regulated by fos remain to be identified. Similar signaling pathways are also activated in response to OS (6–8) and in the context of lysosomal storage disease (LSD; spin is a model of LSD). Antioxidant and autophagic responses are known to be transcriptionally activated by OS via JNK/AP-1 (8, 9). In LSD, lysosomal accumulation generates OS, inducing autophagy, potentially via JNK/AP-1 activation. Increasing autophagy creates an additional burden on lysosomes, generating additional OS. OS and autophagy may regulate synapse growth and structure by damage and phagocytosis of adhesion molecules, contributing to synaptic growth dysregulation (10, 11).

1. Sanyal S, Sandstrom DJ, Hoeffer CA, Ramaswami M (2002) AP-1 functions upstream of CREB to control synaptic plasticity in *Drosophila*. *Nature* 416:870–874.
2. Sanyal S, Narayanan R, Consoulas C, Ramaswami M (2003) Evidence for cell autonomous AP1 function in regulation of *Drosophila* motor-neuron plasticity. *BMC Neurosci* 4:20.
3. Collins CA, Wairkar YP, Johnson SL, DiAntonio A (2006) Highwire restrains synaptic growth by attenuating a MAP kinase signal. *Neuron* 51:57–69.
4. Massaro CM, Pielage J, Davis GW (2009) Molecular mechanisms that enhance synapse stability despite persistent disruption of the spectrin/ankyrin/microtubule cytoskeleton. *J Cell Biol* 187:101–117.
5. Shen W, Ganetzky B (2009) Autophagy promotes synapse development in *Drosophila*. *J Cell Biol* 187:71–79.
6. Wang MC, Bohmann D, Jasper H (2003) JNK signaling confers tolerance to oxidative stress and extends lifespan in *Drosophila*. *Dev Cell* 5:811–816.
7. Saitoh M, et al. (1998) Mammalian thioredoxin is a direct inhibitor of apoptosis signal-regulating kinase (ASK) 1. *EMBO J* 17:2596–2606.
8. Wu H, Wang MC, Bohmann D (2009) JNK protects *Drosophila* from oxidative stress by trancriptionally activating autophagy. *Mech Dev* 126:624–637.
9. Jegga AG, Schneider L, Ouyang X, Zhang J (2011) Systems biology of the autophagy-lysosomal pathway. *Autophagy* 7:477–489.
10. Rowland AM, Richmond JE, Olsen JG, Hall DH, Bamber BA (2006) Presynaptic terminals independently regulate synaptic clustering and autophagy of GABAA receptors in *Caenorhabditis elegans*. *J Neurosci* 26:1711–1720.
11. Bamber BA, Rowland AM (2006) Shaping cellular form and function by autophagy. *Autophagy* 2:247–249.

Table S1. Genotypes and data for normalization of bouton numbers and muscle surface area

Genotype and conditions	Raw bouton no. ± SEM	MSA ± SEM	Normalized bouton number	*n*
Wild-type	85 ± 3.32	80,801 ± 2,265	85 ± 3.32	16
*spin*GAL4 > UAS*trx*^{CYTO}	78 ± 2.9			10
*spin*GAL4 > UAS*hSOD1*	90 ± 4.12			24
*spin*GAL4 > UAS*cat*	76 ± 4.6			18
spin^{4}/*spin*^{5}	152 ± 4.33	76,580 ± 2,716	165 ± 10.3	32
spin^{4}/*spin*^{5} with *spin*GAL4 > UAS*trx*^{CYTO}	113 ± 8.3			10
spin^{4}/*spin*^{5} with *spin*GAL4 > UAS*hSOD1*	110 ± 3.7			46
spin^{4}/*spin*^{5} with *spin*GAL4 > UAS*cat*	103 ± 5.9			17
sod1^{n1}/*sod1*^{n64}	107 ± 4.8	60,421 ± 4,218	147 ± 6.31	21
sod2$^{\Delta}$/*sod2*$^{\Delta 02}$	107 ± 4.9	62,477 ± 3,136	146 ± 10.3	22
sod1$^{n1/+}$	100 ± 3.2	78,550 ± 3,655	103 ± 4.42	18
sod1$^{n64/+}$	87 ± 5.72	76,112 ± 2,544	92 ± 4.31	25
spin$^{5/+}$	85 ± 3.66	75,229 ± 2,665	91 ± 6.49	12
spin$^{4/+}$	93 ± 4.00	80,008 ± 2,321	94 ± 4.10	31
spin$^{5/+}$; *sod1*$^{n1/+}$	121 ± 3.89	75,440 ± 2,355	130 ± 6.29	24
spin$^{4/+}$; *sod1*$^{n1/+}$	114 ± 4.39	72,512 ± 4,565	127 ± 5.47	19
spin$^{5/+}$; *sod1*$^{n64/+}$	137 ± 3.87	78,594 ± 2,157	141 ± 6.14	28
spin$^{4/+}$; *sod1*$^{n64/+}$	116 ± 7.3	71,662 ± 6,982	131 ± 8.03	21
*spin*GAL4 > UAS*jun*^{DN}	64 ± 3.24	73,243 ± 3,578	76 ± 7.02	18
*spin*GAL4 > UAS*fos*^{DN}	56 ± 2.29	75,297 ± 3,820	65 ± 6.25	18
*spin*GAL4 > UAS*jnk*^{DN}	75 ± 3.31	76,823 ± 2,152	79 ± 3.83	23
*spin*GAL4 > UAS*ask*^{DN}	60 ± 4.18	79,476 ± 4,102	61 ± 4.66	15
spin^{4}/*spin*^{5} with *spin*GAL4 > UAS*jun*^{DN}	148 ± 7.19			22
spin^{4}/*spin*^{5} with *spin*GAL4 > UAS*fos*^{DN}	74 ± 1.92			19
spin^{4}/*spin*^{5} with *spin*GAL4 > UAS*jnk*^{DN}	117 ± 5.79			16
spin^{4}/*spin*^{5} with *spin*GAL4 > UAS*ask*^{DN}	128 ± 6.37			16
sod1^{n1}/*sod1*^{n64} with *spin*GAL4 > UAS*jun*^{DN}	104 ± 3.69	69,466 ± 2,060	122 ± 3.88	18
sod1^{n1}/*sod1*^{n64} with *spin*GAL4 > UAS*fos*^{DN}	59 ± 3.70	71,978 ± 2,063	67 ± 4.62	21
sod2$^{\Delta}$/*sod2*$^{\Delta 02}$ *spin*^{5} with *spin*GAL4 > UAS*jun*^{DN}	72 ± 3.77	59,037 ± 3,609	102 ± 5.51	20
sod2$^{\Delta}$/*sod2*$^{\Delta 02}$ *spin*^{5} with *spin*GAL4 > UAS*fos*^{DN}	65 ± 4.25	76,877 ± 2,881	70 ± 5.98	23
sod2$^{\Delta}$/*sod2*$^{\Delta 02}$ *spin*^{5} with *spin*GAL4 > UAS*jnk*^{DN}	84 ± 4.28	73,878 ± 2,423	94 ± 6.30	19
atg1^{PZ}/*atg1*^{DG}	60 ± 3.23			19
atg18^{KG}/*Df*	54 ± 3.96			28
atg18^{KG} /*atg1*^{DG}	68 ± 6.34			28
spin^{4}/*spin*^{5} with *atg1*^{PZ}/*atg1*^{DG}	72 ± 4.90			28
spin^{4}/*spin*^{5} with *atg18*^{KG}/*Df*	75 ± 6.74			16
spin^{4}/*spin*^{5} with *atg18*^{KG}/*atg1*^{DG}	76 ± 5.83			16
*MHC*GAL4 > UAS*hSOD1*	83 ± 6.37			15
spin^{4}/*spin*^{5} with *MHC*GAL4 > UAS*hSOD1*	103 ± 3.166			14
*elav*GAL4 > UAS*hSOD1*	79 ± 4.02			16
spin^{4}/*spin*^{5} with *elav*GAL4 > UAS*hSOD1*	106 ± 7.99			14
*MHC*GAL4 > UAS*fos*^{DN}	79 ± 3.68			22
spin^{4}/*spin*^{5} with *MHC*GAL4 > UAS*fos*^{DN}	120 ± 8.42			11
*elav*GAL4 > UAS*fos*^{DN}	68 ± 3.31			20
spin^{4}/*spin*^{5} with *elav*GAL4 > UAS*fos*^{DN}	113 ± 9.49			9
*MHC*GAL4 > UAS*atg5RNAi*	98 ± 5.69			16
spin^{4}/*spin*^{5} with *MHC*GAL4 > UAS*atg5RNAi*	126 ± 6.51			16
*elav*GAL4 > UAS*atg5RNAi*	81 ± 4.68			17
spin^{4}/*spin*^{5} with *elav*GAL4 > UAS*atg5RNAi*	127 ± 5.57			16
Wild-type (male)	74 ± 3.21			12
*spin*GAL4 > UAS*hSOD1* (male)	71 ± 2.89			21
hiw (male)	146 ± 5.72			20
hiw with *spin*GAL4 > UAS*hSOD1* (male)	108 ± 5.93			25
Wild-type (no paraquat)	78 ± 2.14	72,313 ± 2,837	78 ± 2.14	28
*spin*GAL4^{-} > UAS*hSOD1* (no paraquat)	76 ± 5.56	75,308 ± 3,996	74 ± 4.13	21
Wild-type (10 mM paraquat)	80 ± 6.64	52,003 ± 2,992	114 ± 8.26	21
*spin*GAL4^{-} > UAS*hSOD1* (10 mM paraquat)	57 ± 2.64	59,332 ± 1,937	72 ± 4.07	41
*spin*GAL4 > UAS*jun*^{DN} (no paraquat)	70 ± 3.50	67,204 ± 2,345	75 ± 4.00	22
*spin*GAL4 > UAS*fos*^{DN} (no paraquat)	55 ± 2.70	62,919 ± 4,115	56 ± 5.77	13
*spin*GAL4 > UAS*jnk*^{DN} (no paraquat)	80 ± 4.48	78,220 ± 3,408	75 ± 3.59	22
*spin*GAL4 > UAS*ask*^{DN} (no paraquat)	54 ± 3.64	81,124 ± 2,338	63 ± 4.45	16
*spin*GAL4 > UAS*jun*^{DN} (10 mM paraquat)	56 ± 1.93	64,242 ± 1,950	65 ± 2.64	55
*spin*GAL4 > UAS*fos*^{DN} (10 mM paraquat)	58 ± 2.23	57,525 ± 2,346	75 ± 5.26	19

Table S1. Cont.

Genotype and conditions	Raw bouton no. ± SEM	MSA ± SEM	Normalized bouton number	*n*
*spin*GAL4 > UAS*jnk*^{DN} (10 mM paraquat)	64 ± 3.92	64,026 ± 4,759	76 ± 4.49	17
*spin*GAL4 > UAS*ask*^{DN} (10 mM paraquat)	86 ± 7.80	59,207 ± 5,602	86 ± 7.81	19
*spin*GAL4 > UAS*fos*^{RNAi}	82 ± 4.24			17
spin^{4}/*spin*^{5} with *spin*GAL4 > UAS*fos*^{RNAi}	119 ± 3.81			16
*spin*GAL4 > UAS*jnk*^{RNAi}	65 ± 3.44			22
spin^{4}/*spin*^{5} with *spin*GAL4 > UAS*jnk*^{RNAi}	121 ± 3.45			19

MSA, muscle surface area.

Table S2. Genotypes and data for quantitation of synaptic branching

Genotype	Branch no. ± SEM	Branch no. normalized to bouton no. ± SEM	Branch no. normalized to MSA ± SEM	*n*
Wild-type	5.31 ± 0.44	5.31 ± 0.44	5.31 ± 0.44	16
spin^{4}/*spin*^{5}	10.82 ± 1.33	6.05 ± 0.75	5.54 ± 1.96	11
sod1^{n1}/*sod1*^{n64}	7.19 ± 0.64	5.66 ± 0.50	3.92 ± 1.74	16
sod2$^{\Delta}$/*sod2*$^{\Delta 02}$	3.47 ± 0.32	2.76 ± 0.26	2.01 ± 1.35	17

Table S3. Genotypes and data for quantitation of bouton size

Genotype	Mean bouton width (μm)	*n*	No. NMJs
Wild-type	2.616 ± 0.0638	468	6
spin^{4}/*spin*^{5}	2.350 ± 0.0397	873	5
sod1^{n1}/*sod1*^{n64}	2.202 ± 0.042	610	6
sod2$^{\Delta}$/*sod2*$^{\Delta 02}$	2.646 ± 0.053	551	5